Optimized Design of Distributed Generalized Reed-Solomon Coded Generalized Spatial Modulation

Chunli ZHAO [1], *Fengfan YANG* [2], *Hongjun XU* [3]

[1] College of Information Science and Engineering, Henan University of Technology, Zhengzhou, 450001 China
[2] College of Electronics and Information Engg., Nanjing Univ. of Aeronautics and Astronautics, Nanjing, 210016 China
[3] School of Engineering, University of KwaZulu-Natal, King George V Avenue, Durban, 4041, South Africa

chunlizhao_cn@163.com, yffee@nuaa.edu.cn, xuh@ukzn.ac.za

Submitted February 11, 2025 / Accepted April 4, 2025 / Online first May 6, 2025

Abstract. *To meet the need of modern society for more reliable and efficient communications, this paper applies the generalized spatial modulation (GSM) technique in the distributed generalized Reed-Solomon (GRS) coding to propose a novel distributed GRS coded GSM (DGRSC-GSM) system. In the proposed system, the relay uses the concept of information symbol selection. For different information symbol selections, the destination generates different equivalent linear block codes. To achieve the optimized system design, the optimal information symbol selection (OISS) algorithm by complete search in the relay is proposed to make the destination obtain the best code having the optimal weight distribution. When the GRS codes at the source and relay have large information lengths, the OISS algorithm possesses high complexity. Thus, a low-complexity optimized information symbol selection (LC-OISS) algorithm by incomplete search is put forward. For realizing the effective retrieve of the overall source information, a new joint decoding algorithm in the destination is designed. The results show the superior performance of the proposed DGRSC-GSM system under the OISS and LC-OISS algorithms over that under the random information symbol selection algorithm. Also, the proposed system outperforms the non-cooperative system by 2.6 dB and exhibits more than 2 dB improvement over existing systems.*

Keywords

Generalized Spatial Modulation (GSM), Generalized Reed-Solomon (GRS) codes, distributed channel coding, optimized information symbol selection

1. Introduction

There is an inevitable channel fading phenomenon in wireless communication systems, which seriously affects the system bit error rate (BER) [1]. One effective method to resist channel fading is the cooperative technology whose basic idea is that cooperative nodes share each other's antennas to form a virtual multiple-input multiple-output (MIMO) system that can achieve spatial diversity, thus improving system reliability [2], [3]. The research on cooperative technology originated from Van Der Meulen's analysis of a relay channel model with source (S), relay (R) and destination (D) in [4]. Afterwards, Cover et al. conducted in-depth research on the relay channel in [4] by analyzing the capacity of the relay channel. The ideas of decode-and-forward and amplify-and-forward were introduced in [5], [6]. With the rapid development of wireless communications, the cooperative technology has received widespread attention from both academia and industry, and has been identified as one of the key technologies for the next generation of wireless communication systems by standards such as IEEE 802.11. As compared to the non-cooperative communication transmission, the cooperative communication has obvious advantages: 1) It enhances the ability to resist channel fading and other external interference, thereby improving network service quality; 2) It improves the reliability of communication links, reduces the error probability of transmission channels, and ensures smooth information flow. Due to the superiority of the cooperative communication, it has been applied in the field of cellular network mobile communications. It is worth mentioning that when signals are transmitted in wireless channels, they are also affected by channel additive noise interference in addition to the adverse effects of channel fading. In order to simultaneously combat channel additive noise and channel fading to effectively improve system reliability, Hunter et al. integrated channel coding with cooperative techniques to propose the distributed channel coding or coded cooperative system [7], [8], which can obtain the coding gain and cooperative diversity gain.

Reed-Solomon (RS) codes are non-binary maximum-distance separable (MDS) codes that can correct the maximum number of errors by reaching the minimum distance of the singleton bound (i.e., $n-k+1$) among all linear block codes with equal codeword length n and information length k. Also, RS codes are able to realize a better balance of the system BER and decoding complexity. Due to these advantages of RS codes, the distributed channel coding built by combining cooperative communications and RS

DOI: 10.13164/re.2025.0273

codes has received widespread attention from domestic and foreign researchers. For example, a RS coded cooperative system with adaptive cooperation level in the case of two-source cooperative communications was proposed in [9], where the system adopted a novel algorithm to handle the choice of cooperation level, and had a signal-to-noise ratio (SNR) gain of about 4 dB better than the non-cooperative communication system. A distributed RS coding system for two-source cooperative communications was proposed in [10], which divided data into two parts by using arithmetic operations and transmitted each part to the corresponding user. The simulation results in [10] showed that the BER performance of the proposed system was significantly better than that of the punched convolutional coded cooperative system with rate compatibility. The study in [11] investigated a communication system that cascaded RS codes and convolutional codes in two-source cooperative scenarios, which effectively reduced the noise interference.

Note that the above studies about RS coded cooperation do not adopt the idea of optimized coding at the nodes *S* or *R*, so the equivalent linear block code generated at the *D* do not have an optimized weight distribution. Therefore, it is necessary to study a RS coded cooperative system that can achieve the optimized codeword weight distribution in the *D*. Afterwards, a distributed RS coding based on optimized coding was proposed in [12], which mainly obtained an optimized information selection pattern by adopting an effective information symbol selection algorithm at the *R*, and then used this pattern to appropriately select some symbols from the estimated source information symbols. At the *D*, an equivalent linear block code with the optimized weight distribution was generated. In [12], the effectiveness of the optimized method at the *R* had been confirmed through the numerical simulations, which demonstrated the superior BER performance of the optimized system over the traditional systems. Recently, Chen et al. [13] designed an efficient distributed RS coded space-time labelling diversity communication system and properly selected the source estimation information symbols by using the optimized information symbol selection algorithm proposed in [12]. Numerical results showed that the BER performance of the entire coded cooperative system can be improved by using an appropriate information symbol selection method at the *R*.

As an extension of RS codes, generalized Reed-Solomon (GRS) codes [14] are also a special type of MDS code, and can realize the comprise between the decoding complexity and error performance. Furthermore, GRS codes can be constructed through the combination of multiple encoding parameters, providing greater code-design flexibility than RS codes. Therefore, applying GRS codes to cooperative communications can not only obtain the excellent coding gain provided by GRS codes and the cooperative diversity gain brought by cooperative techniques, but also the constructed distributed GRS coding (DGRSC) system has stronger practical value than the distributed RS coding system. Thus, it is very meaningful to conduct in-depth research on the DGRSC system.

The recently developed MIMO technology has effectively improved the communication quality and significantly enhanced the spectral efficiency as compared to the single antenna technology [15], [16]. The MIMO technology is mainly divided into two categories, i.e., spatial multiplexing and spatial diversity. The fundamental concept of spatial multiplexing technology is to transmit multiple independent data streams on the same frequency through multiple subchannels, which can fully utilize multipath components and thereby improve the system transmission rate. A typical spatial multiplexing technology is vertical Bell Labs layered space-time, but this technique introduces severe inter-channel interference [17]. The spatial diversity technology utilizes multiple parallel links to transmit multiple copies of the original data stream. Due to the independent fading experienced by multiple antennas at the receiving end, the spatial diversity technology can effectively resist channel fading, thereby improving system reliability. However, it has the disadvantage of relatively low spectral efficiency. Spatial modulation (SM) as a newly developed MIMO technology can effectively solve the above problems. This is because the technology uses one effective transmit antenna to send the modulated signal at each instant and its transmit antenna index also carries certain information, which can not only obtain receive diversity but also achieve high spectral efficiency [18–20]. To further improve the spectral efficiency of SM, the concept of generalized spatial modulation (GSM) [18] is proposed. By using multiple activated antennas in GSM to transmit the same modulation symbol, the spatial diversity can be attained. Moreover, this methodology leverages the optimized transmit antenna combination (TAC) to convey constellation symbols, thereby enhancing the BER performance.

The introduction of GSM in distributed channel coding results in a system that achieves high reliability while ensuring effectiveness. In addition, by combining GSM with DGRSC, each GRS codeword symbol can be mapped to the GSM transmit signal vector, which can achieve no conversion loss between codeword symbols and GSM signals. To the best of our knowledge, there is no literature recording the research on the fusion of the GSM and DGRSC. Based on this, the system integrating the GSM with DGRSC, i.e., distributed GRS coded GSM (DGRSC-GSM) is proposed to achieve the effective coordination between reliability and spectral efficiency. Crucially, the introduction of an information symbol selection mechanism at the *R* establishes a close relationship between source coding and relay coding, thereby generating high-reliability code at the *D*. This makes the constructed DGRSC-GSM system far more than a mere integration of two existing systems.

The research achievement closest to the system proposed in this article is the RS coded cooperative SM (RSCC-SM) system [20], but there exist four main differences: 1) In terms of encoding strategy, RS codes are used in [20], but the GRS codes which not only possess flexibly adjustable codeword lengths but also offer a richer set of encoding parameter vectors are used in this article; 2) Regarding MIMO technology implementation, the SM technology is employed in [20], but the GSM technique that achieves signal transmission via the effective TAC is used in this article; 3) In the processing phase at the *R*, the random information selection approach is used in [20], but the optimized information symbol selection algorithms that achieve the intelligent screening of source-estimated information symbols are designed in this article; 4) For the joint decoding at the *D*, a novel joint decoding strategy capable of simultaneously recovering the transmitted symbols from both the selected and non-selected positions in the source information symbols is designed in this article, which is different from the smart and naive decoding algorithms in [20]. The main contributions are introduced as follows:

- This paper first proposes the DGRSC-GSM system based on the information symbol selection at the *R*, where the *R* selects some symbols from the estimated source information and encodes the selected symbols to generate an equivalent linear block code at the *D*.
- An optimal information symbol selection (OISS) algorithm by complete search in the *R* is proposed to construct an equivalent linear block code with the best weight distribution at the *D*, thereby achieving the optimized system design.
- When the GRS codes used by the *S* and *R* have large information lengths, the OISS algorithm has high complexity. Therefore, a low-complexity optimized information symbol selection (LC-OISS) algorithm based on incomplete search is proposed.
- At the *D*, a joint decoding algorithm on the basis of the *S* and *R* is proposed to realize the retrieve of the source message.

The organization of this article is as follows. The DGRSC-GSM system with the information symbol selection at the *R* is introduced in Sec. 2. Two optimized information symbol selection algorithms based on complete/incomplete search are proposed in Sec. 3. At the *D*, a joint decoding algorithm based on the *S* and *R* is proposed in Sec. 4. Section 5 performs the BER performance simulation. Section 6 provides a summary of this article.

Notation: Bold lowercase and uppercase letters separately stand for vectors and matrices. Regular letters and italic letters are scalars and variables, respectively. $\lfloor x \rfloor$ and $\lceil x \rceil$ are the maximum integer not greater than *x* and the minimum integer not less than *x*, respectively. C_x^y is the binomial coefficient, $[\cdot]^{\mathrm{T}}$ is the transpose operation, and $CN(x, y)$ refers to the complex Gaussian distribution with the mean *x* and the variance *y*. $|\mathbf{x}|\mathbf{y}|$ is the combination of **x** and **y**. Also, min(·) and max(·) are the minimum and the maximum value functions, respectively. $|A|$ refers to the cardinality of the set *A*.

2. Distributed GRS Coded GSM (DGRSC-GSM) System by Information Selection at the Relay

Figure 1 shows the model of the DGRSC-GSM system with three nodes (i.e., *S*, *R* and *D*), in which the corresponding nodes separately have N_{t}, N_{t}, and N_{r}, antennas. The proposed system in Fig. 1 enhances the previous RSCC-SM system [20] with three key differences: 1) At both the *S* and *R*, the GRS codes and GSM technology replace the RS codes and SM employed in the RSCC-SM system, significantly enhancing the coding design flexibility, improving the transmission spectral efficiency, and realizing the compromise of reliability and complexity; 2) At the *R*, the novel optimized information symbol selection algorithms replace the random selection strategy adopted in the RSCC-SM system, enabling to optimize the codeword weight distribution at the *D* by precise filtering of source estimation information symbols; 3) At the *D*, a new joint decoding algorithm based on the *S* and *R* supersedes the conventional smart/naive algorithm used in the RSCC-SM system, achieving superior decoding performance through joint processing of dual-path received signals. Furthermore, the complete communication process is accomplished through two time slots.

In time slot-1, the bits-to-symbols (B/S) module at the *S* converts the bit sequence **u** over GF(2) into a symbol sequence $\mathbf{f} = [f_0, f_1, \ldots, f_{K_1-1}]$ over GF(2^m). The GRS code is GRS$_1(N_1,K_1,d_1)$ over GF(2^m) ($m = 1,2,\ldots$), where $N_1 \le 2^m - 1$, K_1 and d_1 represent the codeword length, information length and minimum distance, respectively. The corresponding generator matrix is [21]

$$\mathbf{G}_1 = \begin{bmatrix} v_0^{(1)} & v_1^{(1)} & \cdots & v_{N_1-1}^{(1)} \\ v_0^{(1)}\alpha_0^{(1)} & v_1^{(1)}\alpha_1^{(1)} & \cdots & v_{N_1-1}^{(1)}\alpha_{N_1-1}^{(1)} \\ \vdots & \vdots & \cdots & \vdots \\ v_0^{(1)}(\alpha_0^{(1)})^{K_1-1} & v_1^{(1)}(\alpha_1^{(1)})^{K_1-1} & \cdots & v_{N_1-1}^{(1)}(\alpha_{N_1-1}^{(1)})^{K_1-1} \end{bmatrix} \quad (1)$$

where $\alpha_0^{(1)}, \alpha_1^{(1)}, \ldots, \alpha_{N_1-1}^{(1)}$ over GF(2^m) are the unequal elements and $v_0^{(1)}, v_1^{(1)}, \ldots, v_{N_1-1}^{(1)}$ over GF(2^m) are the non-zero elements. After encoding, the codeword symbol sequence is yielded as follows:

$$\begin{aligned} \mathbf{c} &= [c_0, c_1, \ldots, c_{N_1-1}] \\ &= \mathbf{f}\mathbf{G}_1 = [v_0^{(1)}\mathbf{f}(\alpha_0^{(1)}), v_1^{(1)}\mathbf{f}(\alpha_1^{(1)}), \ldots, v_{N_1-1}^{(1)}\mathbf{f}(\alpha_{N_1-1}^{(1)})] \end{aligned} \quad (2)$$

where $c_l \in \mathrm{GF}(2^m)$ ($l = 0, 1, \ldots, N_1 - 1$). The symbols-to-bits (S/B) module converts **c** into the binary bit sequence **e** of length mN_1, where each symbol c_l in **c** is able to be denoted as a length-*m* bit sequence over GF(2). The data

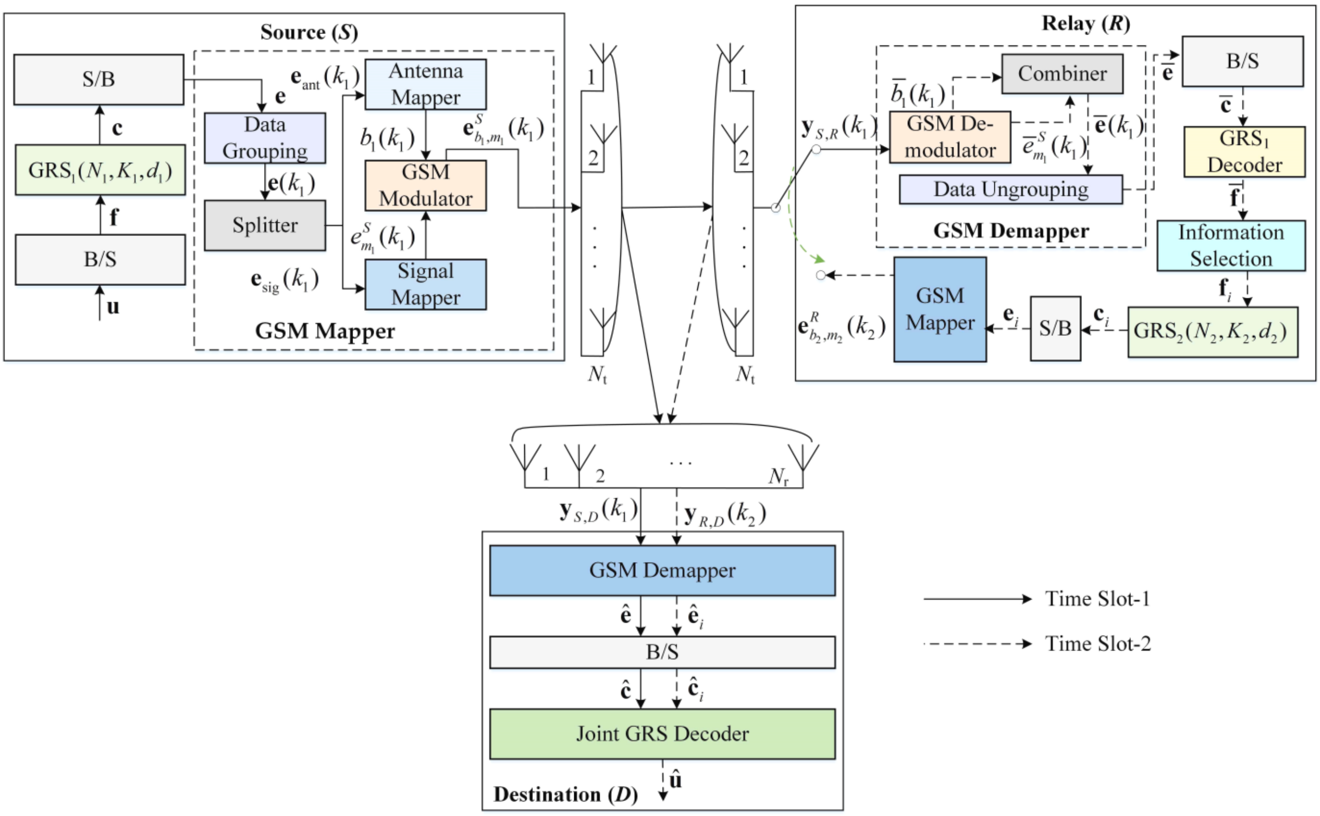

Fig. 1. System model of the DGRSC-GSM.

grouping further divides the sequence $\mathbf{e}$ into some length-m ($m = \log_2\left(\left\lfloor C_{N_t}^{N_u} \right\rfloor\right) + \log_2(M)$) sequences $\mathbf{e}(k_1)$, where M and N_u are separately modulation order and the number of effective transmitting antennas, $k_1 = 1, 2, \ldots, N_1$. In $\mathbf{e}(k_1)$, the sequence $\mathbf{e}_{\text{ant}}(k_1)$ consisting of the first $\log_2\left(\left\lfloor C_{N_t}^{N_u} \right\rfloor\right)$ bits of m bits is used to determine the effective TAC $b_1(k_1) = (b_1^{(1)}(k_1), b_2^{(1)}(k_1), \ldots, b_{N_u}^{(1)}(k_1))$, and the sequence $\mathbf{e}_{\text{sig}}(k_1)$ composed of the remaining $\log_2(M)$ bits is used to get the M-ary quadrature-amplitude modulation (M-QAM) or M-ary phase-shift keying (M-PSK) constellation symbol $e_{m_1}^S(k_1)$ ($m_1 = 1, 2, \ldots, M$). The GSM mapping procedure for GRS codes over the finite field GF(2^4) is in Tab. 1, where binary phase-shift keying (BPSK) is used. The modulated symbol $e_{m_1}^S(k_1)$ is conveyed in the TAC $b_1(k_1)$, and the GSM modulator outputs the transmit vector given by [18]

$$\mathbf{e}_{b_1,m_1}^S(k_1) = [\ldots, 0, e_{m_1}^S(k_1), 0, \ldots, 0, e_{m_1}^S(k_1), 0, \ldots]^{\mathrm{T}}. \tag{3}$$

At the R, the received signal vector $\mathbf{y}_{S,R}(k_1)$ is represented as

$$\begin{aligned} \mathbf{y}_{S,R}(k_1) &= \mathbf{H}_{S,R}\mathbf{e}_{b_1,m_1}^S(k_1) + \mathbf{n}_{S,R}(k_1) \\ &= \mathbf{h}_{S,R}^{b_1(k_1)} e_{m_1}^S(k_1) + \mathbf{n}_{S,R}(k_1) \end{aligned} \tag{4}$$

where $\mathbf{H}_{S,R}$ is the Rayleigh fading channel matrix and $\mathbf{h}_{S,R}^{b_1(k_1)}$ is the sum of the $b_1^{(1)}(k_1)$-th, $b_2^{(1)}(k_1)$-th,..., $b_{N_u}^{(1)}(k_1)$-th columns of $\mathbf{H}_{S,R}$ with all elements being the complex Gaussian random variables with mean 0 and variance 1. $\mathbf{n}_{S,R}(k_1)$ is the noise vector with each element following the complex Gaussian distribution $CN(0,\sigma^2)$.

In time slot-2, the GSM demodulator yields the estimates of $b_1(k_1)$ and $e_{m_1}^S(k_1)$, i.e., $\bar{b}_1(k_1)$ and $\bar{e}_{m_1}^S(k_1)$, respectively. After the combiner and data ungrouping, the estimate $\bar{\mathbf{e}}$ of $\mathbf{e}$ is generated. The GRS decoder performs Euclidean decoding for $\bar{\mathbf{c}}$ from the B/S block to generate the estimation $\bar{\mathbf{f}}$ of $\mathbf{f}$. By adopting information symbol selection, the partial sequence $\mathbf{f}_i = [f_{0,i}, f_{1,i}, \ldots, f_{K_2-1,i}]$ (with length K_2) of $\bar{\mathbf{f}}$ is generated, where i is the selection number. Note that different information symbol selections at the R affect the codeword weight distribution at the D. Next section will provide a detailed introduction to the contents. In the proposed system, the optimized design is achieved by using the optimized information symbol selection at the R. The code GRS$_2$(N_2,K_2,d_2) over GF(2^m) is used with $N_2 \le 2^m - 1$, K_2 and d_2 being the codeword length, information length and minimum distance, respectively. The corresponding generator matrix is [21]

$$\mathbf{G}_2 = \begin{bmatrix} v_0^{(2)} & v_1^{(2)} & \cdots & v_{N_2-1}^{(2)} \\ v_0^{(2)}\alpha_0^{(2)} & v_1^{(2)}\alpha_1^{(2)} & \cdots & v_{N_2-1}^{(2)}\alpha_{N_2-1}^{(2)} \\ \vdots & \vdots & \cdots & \vdots \\ v_0^{(2)}(\alpha_0^{(2)})^{K_2-1} & v_1^{(2)}(\alpha_1^{(2)})^{K_2-1} & \cdots & v_{N_2-1}^{(2)}(\alpha_{N_2-1}^{(2)})^{K_2-1} \end{bmatrix} \tag{5}$$

where $\alpha_{j_1}^{(2)}$ and $v_{j_1}^{(2)}$ ($j_1 = 0,1,\ldots,N_2-1$) are similar to $\alpha_{j_2}^{(1)}$

Field elements	Binary sequences	$N_t = 5$, BPSK	
		Activated TACs	Modulated symbols
0	[0, 0, 0, 0]	(1, 2)	−1
1	[1, 0, 0, 0]	(2, 3)	−1
α	[0, 1, 0, 0]	(1, 4)	−1
α^2	[0, 0, 1, 0]	(1, 3)	−1
α^3	[0, 0, 0, 1]	(1, 2)	+1
α^4	[1, 1, 0, 0]	(3, 5)	−1
α^5	[0, 1, 1, 0]	(1, 5)	−1
α^6	[0, 0, 1, 1]	(1, 3)	+1
α^7	[1, 1, 0, 1]	(3, 5)	+1
α^8	[1, 0, 1, 0]	(2, 4)	−1
α^9	[0, 1, 0, 1]	(1, 4)	+1
α^{10}	[1, 1, 1, 0]	(4, 5)	−1
α^{11}	[0, 1, 1, 1]	(1, 5)	+1
α^{12}	[1, 1, 1, 1]	(4, 5)	+1
α^{13}	[1, 0, 1, 1]	(2, 4)	+1
α^{14}	[1, 0, 0, 1]	(2, 3)	+1

Tab. 1. GSM mapping rule for GRS codes over GF(2^4).

and $v_{j_2}^{(1)}$ ($j_2 = 0,1,...,N_1 - 1$) in (1), respectively. Through encoding, the codeword symbol sequence $\mathbf{c}_i$ of length N_2 is yielded and expressed as

$$\begin{aligned}\mathbf{c}_i &= [c_{0,i}, c_{1,i}, \ldots, c_{N_2-1,i}] \\ &= \mathbf{f}_i \mathbf{G}_2 = [v_0^{(2)} \mathbf{f}_i(\alpha_0^{(2)}), v_1^{(2)} \mathbf{f}_i(\alpha_1^{(2)}), \ldots, v_{N_2-1}^{(2)} \mathbf{f}_i(\alpha_{N_2-1}^{(2)})]\end{aligned} \tag{6}$$

where $c_{l',i} \in \mathrm{GF}(2^m) \quad (l' = 0,1,\ldots, N_2 - 1)$. That S/B module transforms $\mathbf{c}_i$ into binary bit sequence $\mathbf{e}_i$. Next, the GSM mapper maps $\mathbf{e}_i$ into the following transmit vector [18]:

$$\mathbf{e}_{b_2,m_2}^{R}(k_2) = [\ldots, 0, e_{m_2}^{R}(k_2), 0, \ldots, 0, e_{m_2}^{R}(k_2), 0, \ldots]^{\mathrm{T}} \tag{7}$$

where the TAC $b_2(k_2) = (b_1^{(2)}(k_2), b_2^{(2)}(k_2), \ldots, b_{N_u}^{(2)}(k_2))$ is used to transmit the M-QAM/PSK modulated symbol $e_{m_2}^{R}(k_2)$ ($k_2 = 1, 2, \ldots, N_2$, $m_2 = 1, 2, \ldots, M$).

Within their respective time slots, the D acquires the signal vectors from the S and R, with the received signals denoted as follows:

$$\begin{aligned}\mathbf{y}_{S,D}(k_1) &= \mathbf{H}_{S,D} \mathbf{e}_{b_1,m_1}^{S}(k_1) + \mathbf{n}_{S,D}(k_1) \\ &= \mathbf{h}_{S,D}^{b_1(k_1)} e_{m_1}^{S}(k_1) + \mathbf{n}_{S,D}(k_1),\end{aligned} \tag{8}$$

$$\begin{aligned}\mathbf{y}_{R,D}(k_2) &= \mathbf{H}_{R,D} \mathbf{e}_{b_2,m_2}^{R}(k_2) + \mathbf{n}_{R,D}(k_2) \\ &= \mathbf{h}_{R,D}^{b_2(k_2)} e_{m_2}^{R}(k_2) + \mathbf{n}_{R,D}(k_2)\end{aligned} \tag{9}$$

where the Rayleigh fading channel matrices $\mathbf{H}_{S,D}$ and $\mathbf{H}_{R,D}$ are defined similarly to $\mathbf{H}_{S,R}$ in (4), and $\mathbf{n}_{S,D}(k_1)$ and $\mathbf{n}_{R,D}(k_2)$ are defined similarly to $\mathbf{n}_{S,R}(k_1)$ in (4). In addition, $\mathbf{h}_{S,D}^{b_1(k_1)}$ and $\mathbf{h}_{R,D}^{b_2(k_2)}$ are analogous to $\mathbf{h}_{S,R}^{b_1(k_1)}$ in (4). The GSM demapper carries out maximum likelihood detection on the received signals $\mathbf{y}_{S,D}(k_1)$ and $\mathbf{y}_{R,D}(k_2)$ to obtain the estimates $\hat{\mathbf{e}}$ and $\hat{\mathbf{e}}_i$ of the bit sequences $\mathbf{e}$ and $\mathbf{e}_i$. Finally, the joint decoding based on the S and R is used to jointly decode the codeword symbol sequences $\hat{\mathbf{c}}$ and $\hat{\mathbf{c}}_i$ from the B/S block to obtain an estimate $\hat{\mathbf{u}}$ of message bit sequence $\mathbf{u}$ at the S. The details of new joint decoding is introduced in Sec. 4.

3. Novel Optimized Information Symbol Selection Algorithms by Complete/Incomplete Search at the Relay

The R selects the symbol sequence $\mathbf{f}_i$ (i = 1, 2, …, L) of length K_2 from the source estimation information symbol sequence $\overline{\mathbf{f}}$ with length K_1, and there are $L = C_{K_1}^{K_2}$ selection patterns. The i-th choice will make the D generate an equivalent linear block code given by

$$\begin{aligned}&C_D^{(i)}(N_1 + N_2, K_1) \\ &= \left\{ |\,\mathbf{c}\,|\,\mathbf{c}_i\,| \,\middle|\, \mathbf{c} \in \mathrm{GRS}_1(N_1, K_1, d_1), \mathbf{c}_i \in \mathrm{GRS}_2(N_2, K_2, d_2) \right\}.\end{aligned} \tag{10}$$

Assume the codewords $|\,\mathbf{c}\,|\,\mathbf{c}_i\,|$ of weight $\mathrm{wt}(|\,\mathbf{c}\,|\,\mathbf{c}_i\,|) = w$ ($d_{\min}^{(i)} \le w \le N_1 + N_2$) have the number $B_w^{(i)}$, and then the codeword weight distribution under the i-th selection is $1, B_{d_{\min}^{(i)}}^{(i)}, B_{d_{\min}^{(i)}+1}^{(i)}, \ldots, B_{N_1+N_2}^{(i)}$, where $d_{\min}^{(i)}$ is the minimum distance of the code $C_D^{(i)}(N_1 + N_2, K_1)$. When the R adopts the random information symbol selection (RISS) algorithm, it is easy to generate a code with poor weight distribution at the D. Thus, designing an effective information symbol selection algorithm at the R to determine the optimized selection pattern becomes very vital. This section proposes two optimized information symbol selection algorithms at the R.

3.1 Optimal Information Symbol Selection (OISS) Algorithm Based on Complete Search

In order to make the D obtain a code having the best weight distribution, this OISS algorithm based on complete search at the R is proposed, which considers all 2^{mK_1} information symbol sequences over GF(2^m) at the S and determines the optimal selection pattern from all $L = C_{K_1}^{K_2}$ selection patterns at the R.

In the process of determining the optimal selection pattern, the minimum distance (free distance) of the code at the D under different selection patterns is first compared to determine the maximum free distance. If there is only one selection pattern whose minimum distance at the D is equal to the maximum free distance, the corresponding codeword weight distribution at the *D* is optimal and the unique selection pattern is optimal. If the minimum distance of codes in multiple selection patterns is equal to the maximum free distance, the number of minimum distance of codes in these selection patterns is compared: 1) If only one selection pattern generates the smallest number of minimum distance of the codes, the corresponding codeword weight distribution is optimal and this unique selection pattern is the optimal pattern; 2) If multiple selection patterns generate the smallest number of minimum distance of the codes, the number of codewords whose weight is 1 greater than the maximum free distance is further compared. Note that the method for comparing the number of codewords in 2) is similar to the above 1) and 2). If the corresponding selection patterns in 2) are not unique, the cases where the codeword weight is 2, 3, ... greater than the maximum free distance are further considered. The design steps are introduced as follows:

Step 1: Determine all 2^{mK_1} source information symbol sequences. Determine the selection number set $I=\{1,2,\ldots,L\}$ and the following selection pattern set:

$$\begin{aligned}\phi=\{\mathbf{p}_i\mid \mathbf{p}_i=[p_{0,i},p_{1,i},\ldots,p_{K_2-1,i}],\\ 0\le p_{0,i}<p_{1,i}<\ldots<p_{K_2-1,i}\le 1, i\in I\}\end{aligned} \tag{11}$$

where $p_{k,i}$ ($k = 0, 1,\ldots, K_2 - 1$) represents the locations of the symbols selected from that original symbol sequence.

Step 2: For $i \in I$ and $\mathbf{p}_i \in \phi$, determine the free distance of the code at the *D* to obtain the maximum free distance $d_{\min}^{\max}=\max\{d_{\min}^{(i)}\mid i\in I\}$ by considering the corresponding source information symbol sequences in the above step.

Step 3: Determine $I_0=\{i\in I\mid d_{\min}^{(i)}=d_{\min}^{\max}\}$ and $\phi_0=\{\mathbf{p}_i\in\phi\mid i\in I_0\}$.

Step 4: If $|\phi_0|=|I_0|=1$, the entire algorithm is terminated. The unique codeword weight distribution $1,B^{(i)}_{d^{(i)}_{\min}},B^{(i)}_{d^{(i)}_{\min}+1},\ldots,B^{(i)}_{N_1+N_2}$ is optimal and the corresponding selection pattern (i.e. the unique element in ϕ_0) is the optimal one $\mathbf{p}^{(\mathrm{opt})}$.

Step 5: If $|\phi_0|=|I_0|\neq 1$, set $t=0$.

(i) For $i\in I_t$ and $\mathbf{p}_i\in\phi_t$, find the number $B^{(i)}_{d_{\min}^{\max}}$ of codeword weight $d_{\min}^{\max}$ at the *D*, and then determine $B^{\min}_{d_{\min}^{\max}}=\min\{B^{(i)}_{d_{\min}^{\max}}\}$, $I_{t+1}=\{i\in I_t\mid B^{(i)}_{d_{\min}^{\max}}=B^{\min}_{d_{\min}^{\max}}\}$ and $\phi_{t+1}=\{\mathbf{p}_i\in\phi_t\mid i\in I_{t+1}\}$.

(ii) If $|\phi_{t+1}|=|I_{t+1}|=1$, the unique codeword weight distribution $1,B^{(i)}_{d^{(i)}_{\min}},B^{(i)}_{d^{(i)}_{\min}+1},\ldots,B^{(i)}_{N_1+N_2}$ $(i\in I_{t+1})$ is optimal and take the corresponding selection pattern (the unique element in ϕ_{t+1}) as the best one $\mathbf{p}^{(\mathrm{opt})}$; If $d_{\min}^{\max}<N_1+N_2$ and $|\phi_{t+1}|=|I_{t+1}|\neq 1$, set $t\leftarrow t+1$ and $d_{\min}^{\max}\leftarrow d_{\min}^{\max}+1$, and then go back to step (i); If $d_{\min}^{\max}=N_1+N_2$, any codeword weight distribution $1,B^{(i)}_{d^{(i)}_{\min}},B^{(i)}_{d^{(i)}_{\min}+1},\ldots,B^{(i)}_{N_1+N_2}$ under $i\in I_{t+1}$ can be used as the optimal codeword weight distribution, and any pattern in ϕ_{t+1} is taken as the best one $\mathbf{p}^{(\mathrm{opt})}$.

3.2 Low-Complexity Optimized Information Symbol Selection (LC-OISS) Algorithm Based on Incomplete Search

The OISS algorithm considers all 2^{mK_1} source information symbol sequences and selects one pattern from the total $L=C_{K_1}^{K_2}$ selection patterns to make the *D* generate a code having the optimal codeword weight distribution. When $\mathrm{GRS}_1(N_1,K_1,d_1)$ and $\mathrm{GRS}_2(N_2,K_2,d_2)$ have large information lengths, the search has high complexity. Since the codeword generated by the information sequence $\mathbf{f}$ is $\mathbf{c}=[v_0^{(1)}\mathbf{f}(\alpha_0^{(1)}),v_1^{(1)}\mathbf{f}(\alpha_1^{(1)}),\ldots,v_{N_1-1}^{(1)}\mathbf{f}(\alpha_{N_1-1}^{(1)})]$ at the *S*, the polynomial $\mathbf{f}(x)$ has $N_1'=N_1-\varpi$ different roots in $\boldsymbol{\alpha}_1=[\alpha_0^{(1)},\alpha_1^{(1)},\ldots,\alpha_{N_1-1}^{(1)}]$ of length N_1 for $\mathrm{wt}(\mathbf{c})=\varpi$ ($d_1\le\varpi\le N_1$), and $J-N_1'$ roots in the remaining elements of GF(2^m) except for $\boldsymbol{\alpha}_1$, where *J* is the possible largest degree of $\mathbf{f}(x)$. By randomly and fixedly selecting *J* elements from GF(2^m) as the roots of $\mathbf{f}(x)$, partial information sequences of 2^{mK_1} source information symbol sequences can be effectively obtained. In addition, the K_1 source estimation information symbols are approximately evenly divided into the two parts from which the K_2 symbols are selected in reasonable ways. In each scenario, the locations of the K_2 symbols selected from that original K_1 source estimation information symbols form a selection pattern. The partial patterns of *L* selection patterns are effectively obtained by considering multiple scenarios.

To mitigate the computational complexity of the OISS algorithm while identifying a selection pattern that induces an optimized codeword weight distribution in the *D*, a LC-OISS algorithm that only considers partial (K_b) sequences of 2^{mK_1} source information symbol sequences and partial (*P*) patterns of *L* selection patterns is proposed, where $K_\mathrm{b}<2^{mK_1}$ and $P<L$. The details are as follows:

Step 1: Determine K_b source information symbol sequences.

(i) Partition all 2^m elements of GF(2^m) into two parts, as depicted in Fig. 2.

(ii) Select *J* elements from the 2^m elements of GF(2^m) as all roots of $\mathbf{f}(x)$. a) N_1' elements of *J* elements are chosen in the 1st portion of Fig. 2. Specifically, i) the 1st part is partitioned into two almost equal parts (i.e., the 1st$^{(1)}$ part and the 1st$^{(2)}$ part), where the 1st$^{(1)}$ part is composed of the first $\lceil (N_1+1)/2\rceil$ elements (more elements) in the 1st part and the 1st$^{(2)}$ part is composed of the remaining $N_1-\lceil (N_1+1)/2\rceil$ elements in

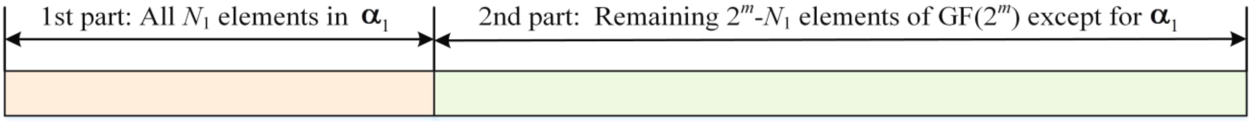

Fig. 2. Division of 2^m elements in GF(2^m).

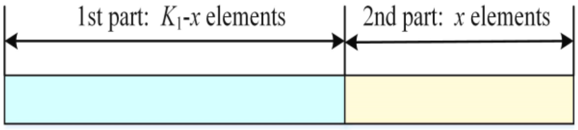

Fig. 3. Division of K_1 source estimation information symbols.

the 1st part; ii) more elements (i.e., $\bar{x}$ elements) are randomly chosen from the 1st$^{(1)}$ part, whereas the remaining $N_1' - \bar{x}$ elements are fixedly selected in the 1st$^{(2)}$ portion to get $C^{\bar{x}}_{\lceil (N_1+1)/2 \rceil}$ cases, where $\lceil (N_1'+1)/2 \rceil \le \bar{x} \le \min(N_1', \lceil (N_1+1)/2 \rceil)$. b) The remaining $J - N_1'$ elements are chosen in the 2nd portion of Fig. 2. The specific selection method is similar to a) and yields $C^{\bar{\bar{x}}}_{\lceil (2^m - N_1+1)/2 \rceil}$ cases, where $\lceil (J - N_1'+1)/2 \rceil \le \bar{\bar{x}} \le \min(J - N_1', \lceil (2^m - N_1+1)/2 \rceil)$.

(iii) At the S, the K_b information symbol sequences are obtained by considering the $C^{\bar{x}}_{\lceil (N_1+1)/2 \rceil} + C^{\bar{\bar{x}}}_{\lceil (2^m - N_1+1)/2 \rceil}$ scenarios.

Step 2: Determine P selection patterns.

(i) Based on the value of $\lfloor K_1 / K_2 \rfloor$, the K_1 source estimation information symbols are divided into two parts as shown in Fig. 3, where the parameter x has the following expression form:

$$x = \begin{cases} \lceil (K_1+1)/2 \rceil & \text{if } \lfloor K_1/K_2 \rfloor = 1 \\ \lfloor (K_1-1)/2 \rfloor & \text{if } \lfloor K_1/K_2 \rfloor > 1 \end{cases}. \tag{12}$$

Through this way, the K_1 source estimation information symbols can be approximately evenly divided.

(ii) From the K_1 source information symbols, the K_2 symbols are chosen. a) For $\lfloor K_1 / K_2 \rfloor = 1$, it means that there exist a relatively larger number of symbols selected from the K_1 symbols, and therefore more symbols are chosen from the 2nd part (with more elements) in Fig. 3. Specifically, randomly select z ($\lceil (K_2 + 1)/2 \rceil \le z \le \min(K_2, x)$) symbols from the 2nd part of Fig. 3 and fixedly select $K_2 - z$ symbols from the 1st part of Fig. 3, which generates C^z_x cases. b) For $\lfloor K_1 / K_2 \rfloor > 1$, it means that the number of selected symbols from K_1 symbols is relatively small, and therefore fewer symbols are selected from the 2nd part (with fewer elements) in Fig. 3. Specifically, $\bar{z}$ ($0 \le \bar{z} \le \min(\lfloor (K_2 - 1)/2 \rfloor, x)$) symbols are randomly selected from the 2nd part of Fig. 3, and fixedly select $K_2 - \bar{z}$ symbols from the 1st part of Fig. 3, which generates $C^{\bar{z}}_x$ cases.

(iii) The locations of the K_2 symbols chosen from that source estimation information sequence $\bar{\mathbf{f}}$ for each case constitute a selection pattern at the R. By considering all the possible $C^z_x + C^{\bar{z}}_x$ cases, the P selection patterns $\bar{\mathbf{p}}_1, \bar{\mathbf{p}}_2, \ldots, \bar{\mathbf{p}}_P$ at the R are further determined.

Step 3: Based on the generated P selection patterns in the above step 2, $\bar{I} = \{1, 2, \ldots, P\}$ and $\bar{\phi} = \{\bar{\mathbf{p}}_1, \bar{\mathbf{p}}_2, \ldots, \bar{\mathbf{p}}_P\}$ are further obtained.

Step 4: Follow steps 2-5 in the OISS to perform the remaining steps. At last, from the determined P selection patterns in the above step 3, an optimized one $\mathbf{p}^{(\text{low})} = \bar{\mathbf{p}}_{\bar{i}}$ ($\bar{i} \in \bar{I}$) is selected.

4. Joint Decoding at the Destination on the Basis of the Source and Relay

In the proposed DGRSC-GSM system (see Fig. 1), the D generates a code different from the GRS code, so the idea that uses the decoding algorithm of the GRS code to decode the received signal is not feasible. As we all know, maximum likelihood decoding can easily lead to higher complexity. Thus, it is vital to propose a joint decoding algorithm that achieves a good compromise between the complexity and performance. The code GRS$_2$(N_2, K_2, d_2) at the R has stronger error correction ability as compared to the code GRS$_1$(N_1, K_1, d_1) in the S. At the D, a joint decoding algorithm on the basis of the S and R is proposed to acquire the source message and the specific decoding process is shown in Fig. 4. This decoding algorithm obtains effective estimation of length-K_1 source information by achieving high reliability of corresponding symbols located at $K_1 - K_2$ unselected positions in the source estimation information symbols, and effective replacement of relay estimation information symbols in the K_2 selected positions of the source estimation information symbols. The details are as follows:

Step 1: The GRS$_2$ decoder first performs Euclidean decoding on $\hat{\mathbf{c}}_i$ to obtain a reliable estimate $\hat{\mathbf{f}}_i$ of the relay information symbol sequence $\mathbf{f}_i$ with length K_2.

Step 2: By using the zero padding block, the sequence $\hat{\mathbf{f}}_i$ is updated as a new sequence $\bar{\bar{\mathbf{f}}}$ with length K_1, where $\hat{\mathbf{f}}_i$ is located at the selected K_2 positions. By using the GRS$_1$ encoder, the sequence $\bar{\bar{\mathbf{f}}}$ is encoded into the codeword symbol sequence $\bar{\bar{\mathbf{c}}} = \bar{\bar{\mathbf{f}}}\,\mathbf{G}_1$ with length N_1.

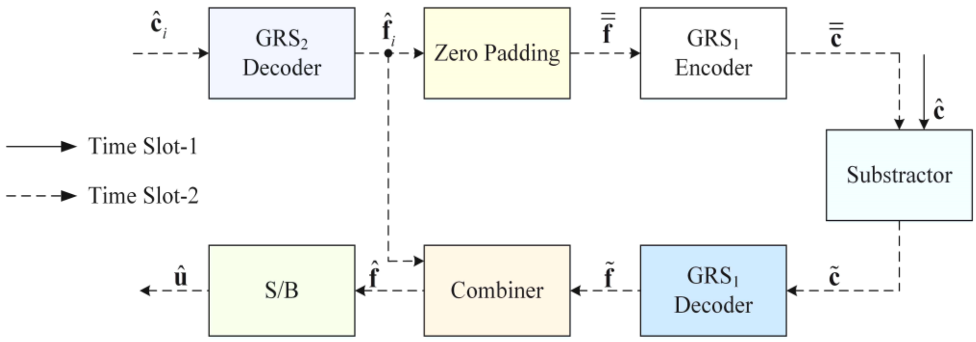

Fig. 4. Joint decoding at the *D*.

Step 3: Obtain the updated sequence $\tilde{\mathbf{c}} = \hat{\mathbf{c}} - \bar{\bar{\mathbf{c}}}$ of $\hat{\mathbf{c}}$ by sending the sequences $\hat{\mathbf{c}}$ and $\bar{\bar{\mathbf{c}}}$ to the subtractor, which makes the sequence $\tilde{\mathbf{c}}$ has higher reliability than $\hat{\mathbf{c}}$ due to the lower dimension of the code space composed of all codewords $\tilde{\mathbf{c}}$ compared to the code space composed of all codewords $\hat{\mathbf{c}}$. Then, GRS_1 decoder decodes $\tilde{\mathbf{c}}$ to output the reliable estimate $\tilde{\mathbf{f}}$ of the source information symbol sequence $\mathbf{f}$ with length K_1.

Step 4: Due to the stronger error correction ability of the GRS code used by the *R* compared to the GRS code used by the *S*, the symbol sequence $\hat{\mathbf{f}}_i$ with higher reliability is used to replace the symbols located at K_2 selected positions in the sequence $\tilde{\mathbf{f}}$ through the combiner. Then, the updated sequence $\hat{\mathbf{f}}$ of $\tilde{\mathbf{f}}$ is further obtained, which is utilized as the final estimation of this source message symbol sequence $\mathbf{f}$.

Step 5: Convert symbol sequence $\hat{\mathbf{f}}$ to bit sequence $\hat{\mathbf{u}}$, which is used as the final estimation of this source message bit vector $\mathbf{u}$.

5. Simulation Results

This section evaluates the performance of the proposed DGRSC-GSM system and its compared systems in the Rayleigh fading channel. For the slow Rayleigh fading channel, the channel matrix remains invariant throughout the transmission duration of individual codewords while exhibiting variation across distinct codeword transmission intervals. The fast Rayleigh fading channel indicates that the corresponding channel matrix for each transmitted GSM vector is different. The parameter used in the slow and fast Rayleigh fading channels is the path gain modeled as a complex Gaussian random variable obeying $CN(0, 1)$. The GRS codes of three cases over GF(q), i.e., $\mathrm{GF}(2^4)=\{0,1, \beta,\ldots,\beta^{14}\}$, $\mathrm{GF}(2^5)=\{0,1, \gamma,\ldots,\gamma^{30}\}$ and $\mathrm{GF}(2^6)=\{0,1, \chi,\ldots,\chi^{62}\}$ are mainly considered, where β, γ and χ are separately the roots of $1 + x + x^4$, $1 + x^2 + x^5$ and $1 + x + x^6$ over GF(2). Table 2 presents the GRS coding parameters under three cases along with the optimized selection patterns. The selection of N_t, N_u and M needs to satisfy $\log_2(q) = \log_2\left(\left\lfloor C_{N_\mathrm{t}}^{N_\mathrm{u}} \right\rfloor\right) + \log_2(M)$ and $N_\mathrm{r} \le 6$ is selected to facilitate receive antenna configuration. The detection is maximum-likelihood to perform optimal detection. The decoding algorithm of GRS codes is effective and simple Euclidean decoding algorithm whose core idea lies in repeatedly performing polynomial division $r_{i+1}(x) = r_{i-1}(x) - q_i(x) r_i(x)$ $(i \ge 1)$ to get the error-location polynomial and error-value evaluator. The corresponding initial criteria is $r_0(x) = x^{2t}$ and $r_1(x) = S(x)$, where t is the error correction capability and $S(x)$ is the syndrome polynomial.

The assumption of the ideal *S*-*R* channel ($\lambda_{S,R} = \infty$) and perfect channel knowledge depends on two aspects: 1) The time consumption of the simulations is reduced; 2) The inherent relationship between the system parameters and BER performance is easily observed. For emulate real-word scenarios, the performance under the non-ideal *S*-*R* channel ($\lambda_{S,R} \neq \infty$) or imperfect channel knowledge is also implemented. The *R* is deployed closer to the *D*, enabling the *R*-*D* channel to obtain 2 dB SNR gain per symbol over the *S*-*D* channel, i.e., $\lambda_{R,D} = \lambda_{S,D} + 2$. The simulations are performed in a MATLAB environment. The curves show the relationship between the BER and SNR ($\lambda_{S,D}$) of the *S*-*D* channel. It should be noted that all other subsections except for Sec. 5.8 consider the slow Rayleigh fading channel.

Cases	$\mathbf{GRS_1(N_1, K_1, d_1)}$ $\mathbf{GRS_2(N_2, K_2, d_2)}$	Optimized selection patterns
1	$\mathrm{GRS}_1(12, 5, 8)$ $\mathrm{GRS}_2(12, 3, 10)$	$\mathbf{p}^{(\mathrm{opt})}=[1, 3, 5]$, $\mathbf{p}^{(\mathrm{low})}=[1, 2, 5]$
2	$\mathrm{GRS}_1(31, 19, 13)$ $\mathrm{GRS}_2(31, 10, 22)$	$\mathbf{p}^{(\mathrm{low})}=[1, 2, 3, 4, 6, 7, 11, 12, 13, 17]$
3	$\mathrm{GRS}_1(63, 50, 14)$ $\mathrm{GRS}_2(63, 30, 34)$	$\mathbf{p}^{(\mathrm{low})}=[1, 3, 4, 5, 6, 7, 8, 9, 10, 11, 12, 15, 16, 20, 25, 26, 27, 28, 29, 30, 31, 32, 34, 35, 43, 46, 47, 48, 49, 50]$

Tab. 2. Optimized selection patterns of three cases.

5.1 Performance of the DGRSC-GSM System with Different Information Symbol Selection Algorithms

Figure 5 shows the BER performance of the DGRSC-GSM system with perfect channel knowledge using various information symbol selection algorithms at the R in case 1 with $N_t = 5$, $N_r = 4$, $N_u = 2$ and $M = 2$ (BPSK), where the S-R channel is ideal ($\lambda_{S,R} = \infty$) and it means that the S-R link is not affected by noise interference. From Fig. 5, it can be seen that the system using the OISS and the LC-OISS algorithms exhibits better BER performance than that using the RISS algorithm. The reason for this phenomenon is that the OISS and LC-OISS algorithms endow the equivalent codes at the D with a larger free distance (i.e., 10) compared to the free distance (i.e., 8) generated by the RISS algorithm, thereby optimizing the weight distribution and further enhancing system performance. At BER = 10^{-5}, the system under the OISS and the LC-OISS algorithms is approximately 2.48 dB and 2.3 dB better than the system under the RISS algorithm, respectively.

In addition, the results in Fig. 5 indicate that the BER performance under the LC-OISS algorithm with the local search is very close to that under the OISS algorithm with the optimal search. This phenomenon occurs because the equivalent free distance (i.e., 10) at the D generated by the LC-OISS algorithm is the same as that generated by the OISS algorithm, but the LC-OISS algorithm only produces a slightly higher number (i.e., 15) of codewords with this free distance compared to the number (i.e., 11) of the free distance generated by the OISS algorithm. As a result, the weight distribution generated by the LC-OISS algorithm exhibits optimized characteristics, thereby leading to improved performance. Thus, for the other two cases in Tab. 2, the optimized selection algorithm is the LC-OISS algorithm and the BER performance under this algorithm is shown in Figs. 6 and 7, where $\lambda_{S,R} = \infty$, $N_t = 3$, 5, $N_r = 4$,

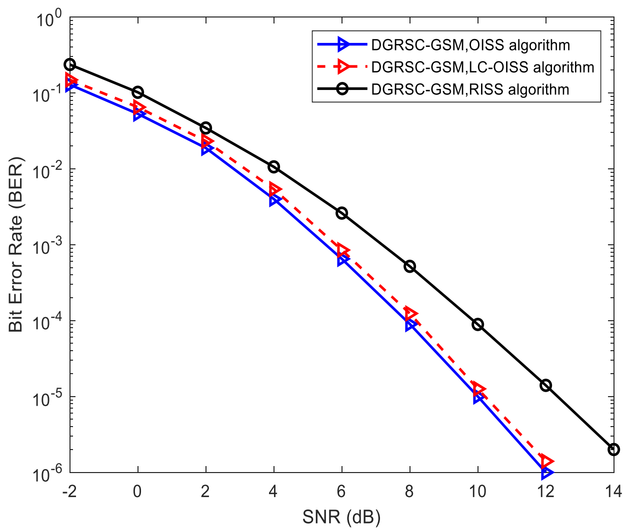

Fig. 5. Performance comparison of the DGRSC-GSM system using $GRS_1(12,5,8)$ and $GRS_2(12,3,10)$ under different information symbol selection algorithms.

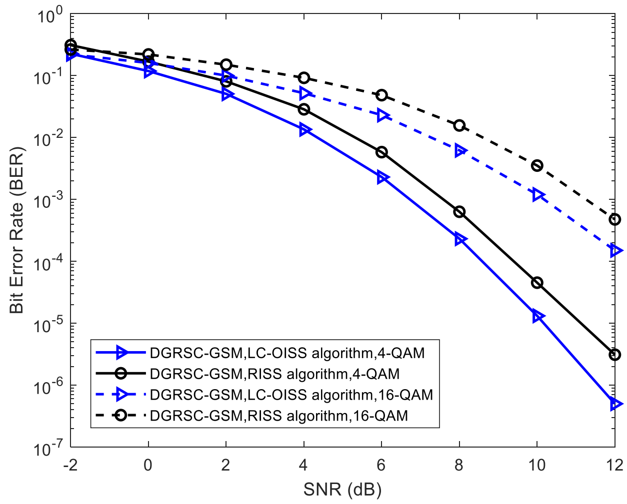

Fig. 6. Performance comparison of the DGRSC-GSM system using $GRS_1(31,19,13)$ and $GRS_2(31,10,22)$ under different information symbol selection algorithms.

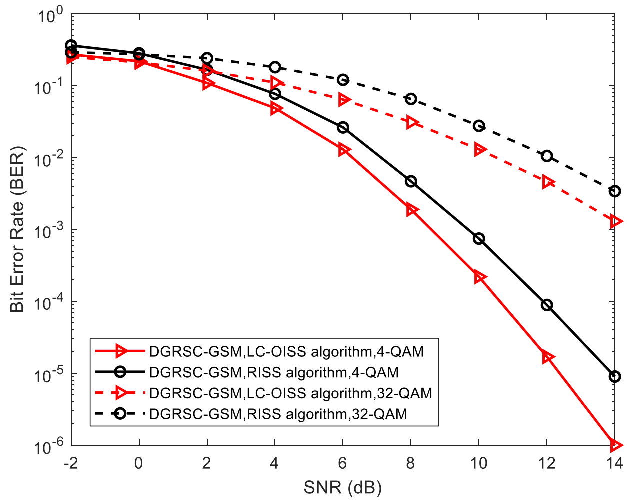

Fig. 7. Performance comparison of the DGRSC-GSM system using $GRS_1(63,50,14)$ and $GRS_2(63,30,34)$ under different information symbol selection algorithms.

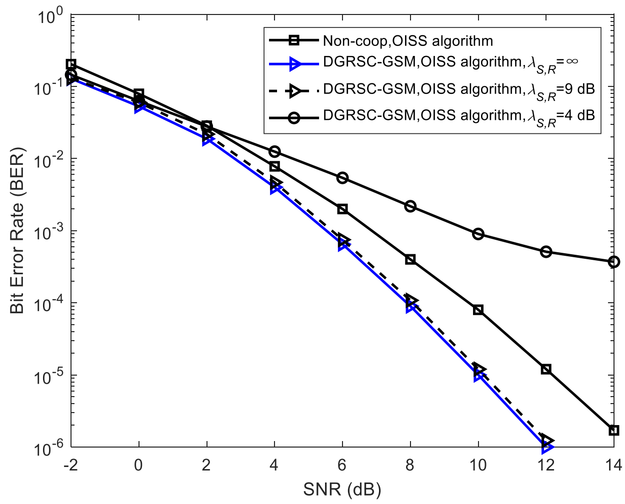

Fig. 8. Performance comparison of the DGRSC-GSM system (using $GRS_1(12,5,8)$ and $GRS_2(12,3,10)$) and its corresponding non-cooperative system.

$N_u = 2$, $M = 16$, 4 (16-QAM, 4-QAM) are used in case 2 and $\lambda_{S,R} = \infty$, $N_t = 3$, 7, $N_r = 4$, $N_u = 2$, $M = 32$, 4 (32QAM, 4-QAM) are utilized in case 3. The performance in Figs. 6 and 7 reconfirms the superiority of the LC-OISS algorithm over the RISS algorithm.

5.2 Performance of the DGRSC-GSM System and Its Non-Cooperative System

Figure 8 shows the performance curves of the DGRSC-GSM system and the corresponding non-cooperative scheme with perfect channel knowledge, where the MIMO figuration (i.e., $N_t = 5$, $N_r = 4$, $N_u = 2$, $M = 2$ (BPSK)) is used and the R uses an OISS algorithm based on global search. In cooperative scenarios, the system performance has been investigated under the non-ideal S-R channel ($\lambda_{S,R} \neq \infty$) and ideal S-R channel ($\lambda_{S,R} = \infty$). The results in Fig. 8 indicate the performance with larger $\lambda_{S,R}$ (such as $\lambda_{S,R} = 9$ dB) under $\lambda_{S,R} \neq \infty$ approaches that under $\lambda_{S,R} = \infty$. However, if $\lambda_{S,R}$ drops to a smaller value (i.e., $\lambda_{S,R} = 4$ dB), the performance also decreases and the error floor occurs. This can be explained by the fact that a higher value of $\lambda_{S,R}$ facilitates superior performance, whereas a lower value of $\lambda_{S,R}$ leads to erroneous decoding at the R and results in performance degradation. The results in Fig. 8 also reveal the DGRSC-GSM system ($\lambda_{S,R} = \infty$ and $\lambda_{R,D} = \lambda_{S,D} + 2$) surpasses the non-cooperative scheme, where this non-cooperative scenario is the cooperative scenario with $\lambda_{S,R} = \infty$ and $\lambda_{S,D} = \lambda_{R,D}$. It is because the SNR of the R-D channel in the cooperative scenarios is higher than that in the non-cooperative scenarios, endowing the proposed cooperative system with superior BER performance. For instance, the cooperative system gets a 2.6 dB gain over non-cooperative counterpart at BER of 1.7×10^{-6}. Figures 9 and 10 reveal a phenomenon similar to Fig. 8. In Fig. 9, $N_t = 5$, $N_r = 4$, $N_u = 2$ and $M = 4$ (4-QAM) are utilized. In Fig. 10, $N_t = 7$, $N_r = 4$, $N_u = 2$ and $M = 4$ (4-QAM) are utilized.

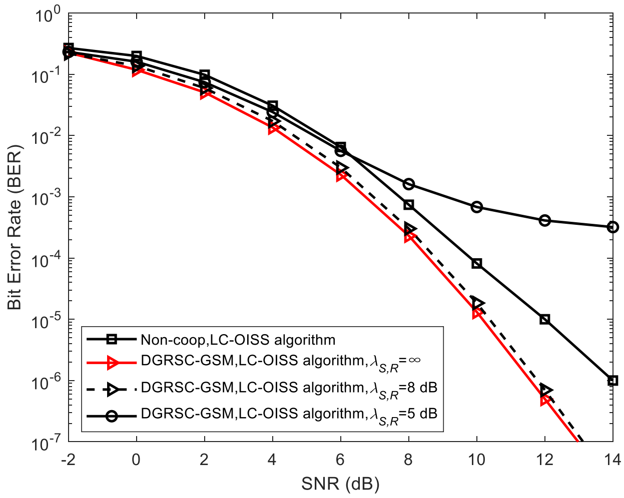

Fig. 9. Performance comparison of the DGRSC-GSM system (using $GRS_1(31,19,13)$ and $GRS_2(31,10,22)$) and its corresponding non-cooperative system.

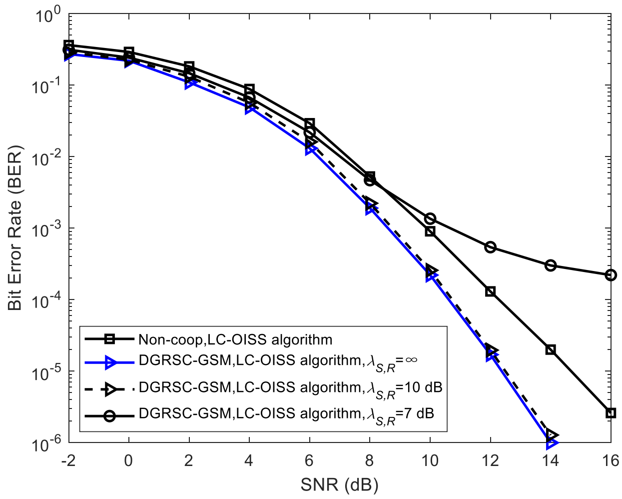

Fig. 10. Performance comparison of the DGRSC-GSM system ($GRS_1(63,50,14)$ and $GRS_2(63,30,34)$) and its corresponding non-cooperative system.

5.3 Performance of the DGRSC-GSM System under Different Receive Antenna Number

The performance impact of different antenna number N_r at the D on the DGRSC-GSM system under $\lambda_{S,R} = \infty$ is also discussed, as shown in Fig. 11, where perfect channel knowledge is assumed, the GRS codes $GRS_1(63, 50, 14)$ and $GRS_2(63, 30, 34)$ are separately used at the S and R, the R adopts a LC-OISS algorithm, $N_t = 7$, $N_u = 2$ and the modulation scheme is 4-QAM ($M = 4$). The simulation results demonstrate that the BER performance is significantly enhanced as the number N_r of receiving antennas increases at the D, which is because the increase of N_r improves the antenna diversity gain.

5.4 Performance Comparison between the DGRSC-GSM System and the Existing Scheme

Additionally, the results demonstrate the performance of the proposed DGRSC-GSM system using $GRS_1(63, 50, 14)$ and $GRS_2(63, 30, 34)$, and the state-of-the-art (SOTA) solutions, i.e., adaptive polar coded cooperation (APCC) [1], Goppa coded cooperation (GCC) [2], RS coded cooperation (RSCC) [12], RSCC-SM [20] and distributed RS codes (DRSC) [22], reconfigurable intelligent surface assisted low-density parity-check coded cooperation (RIS-LDPCCC) [24] and reconfigurable intelligent surface assisted polar coded cooperation (RIS-PCC) [25], as shown in Fig. 12. The perfect channel knowledge and ideal S-R channel are assumed. In order to realize the same spectral efficiency: 1) In the proposed system, $N_t = 7$, $N_u = 2$ and $M = 4$ (4-QAM) are used; 2) In the RSCC-SM system, $N_t = 16$ and $M = 4$ (4-QAM) are utilized; 3) In the APCC, GCC, RSCC, DRSC, RIS-LDPCCC and RIS-PCC systems, $N_t = 1$ and $M = 64$ (64-QAM) are used. For obtaining the identical effective code rate at the *D*: 1) The RS codes $RS_1(63, 50, 14)$ and $RS_2(63, 30, 34)$ are simultaneously assumed in the RSCC, RSCC-SM and DRSC systems; 2) Binary LDPC codes and Goppa codes with an equivalent codeword length of 756 at the *D* are adopted in the RIS-LDPCCC (with 10 reflecting elements) and GCC, respectively; 3) Binary polar codes with an equivalent codeword length of 512 at the *D* are utilized in both the RIS-PCC (with 10 reflecting elements) and APCC. The codeword length of 512 is specifically selected for polar codes as it satisfies the power-of-two constraint required by polar code construction while maintaining proximity to the target length of 756. Furthermore, the DGRSC-GSM, GCC, RSCC, RSCC-SM and DRSC systems adopt Euclidean decoding. The RIS-LDPCCC system uses the belief propagation decoding with 10 iterations. Both the APCC and RIS-PCC systems employ the cyclic redundancy check (CRC) aided successive cancellation list decoding with embedded 16-bit CRC and list size $L = 32$.

The experimental results demonstrate that the proposed concept surpasses the SOTA solutions. This is mainly because the proposed DGRSC-GSM system effectively gets the coding and diversity gains by adopting the GSM technique and optimized GRS coding at the *R*. As shown in Fig. 12, at a BER of 10^{-5}, the proposed system outperforms the existing systems by more than 2 dB.

5.5 Performance Comparison of the DGRSC-GSM and Distributed GRS Coded SM (DGRSC-SM) Systems

Figure 13 exhibits the performance of DGRSC-GSM and DGRSC-SM systems under the ideal *S-R* channel (i.e., $\lambda_{S,R} = \infty$) when the conditions are identical, where the perfect channel knowledge is supposed, the *R* adopts a LC-OISS algorithm based on partial search. To achieve the same spectral efficiency: 1) For DGRSC-GSM with $N_t = 7$ and DGRSC-SM with $N_t = 16$, the modulation scheme is 4-QAM ($M = 4$); 2) For DGRSC-GSM with $N_t = 5$ and DGRSC-SM with $N_t = 8$, the modulation 8-QAM ($M = 8$) is adopted. The results show the BER performance of the DGRSC-SM system is close to that of the proposed DGRSC-GSM system for the identical number N_r of receiving antennas at the *D*.

The complexity difference between the DGRSC-GSM and DGRSC-SM systems lies in the detection complexity at the *D*. During the process of complexity calculations, only addition and multiplication operations are considered. In the DGRSC-GSM system, the detection complexity at the *D* is composed of GSM detection complexity (i.e., $A = (N_1 + N_2)[2^{l_1}(3N_r + M - 1) + M + N_r(N_u - 1)]$) [23] and joint decoding complexity (i.e., $B = 2q(\log_2(q))^2$) [26], where $l_1 = \log_2\left(\left\lfloor C_{N_t}^{N_u} \right\rfloor\right)$. Thus, the total complexity of the DGRSC-GSM system is $A + B$. For the DGRSC-SM system, the overall complexity is represented as $C + B$, where $C = (N_1 + N_2)[N_t(3N_r + M - 1) + M]$ is the SM de-

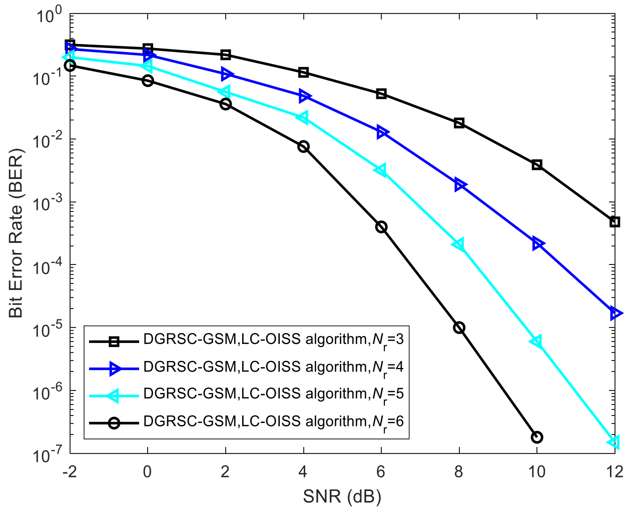

Fig. 11. Performance comparison of the DGRSC-GSM system using $GRS_1(63,50,14)$ and $GRS_2(63,30,34)$ under different receive antenna number N_r.

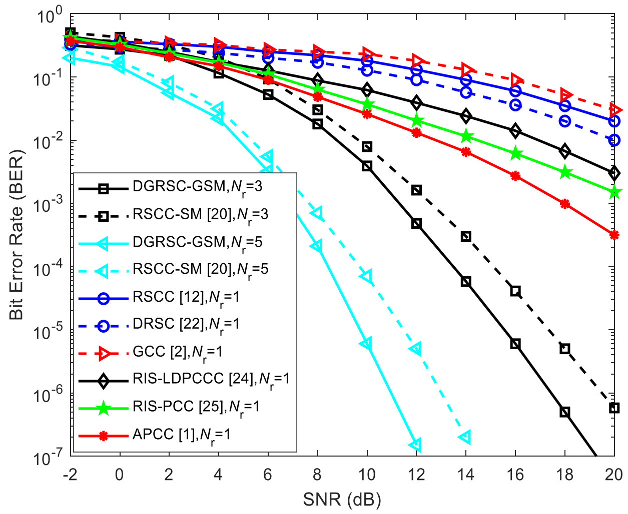

Fig. 12. Performance comparison of the DGRSC-GSM system and the SOTA systems.

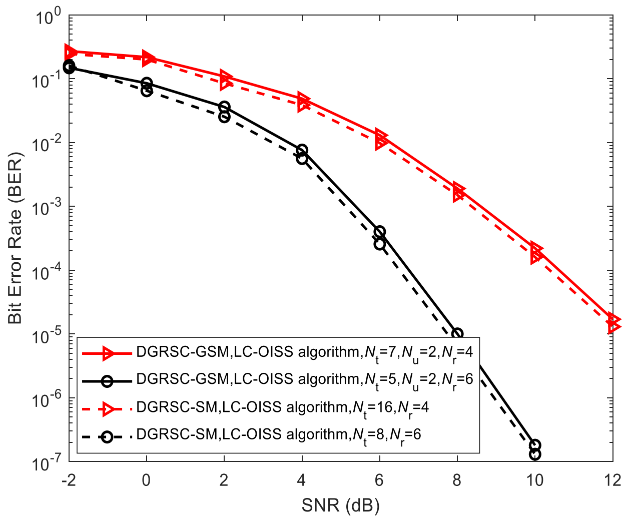

Fig. 13. Performance of the DGRSC-GSM and DGRSC-SM systems using $GRS_1(63,50,14)$ and $GRS_2(63,30,34)$.

tection complexity. For instance, the complexity of DGRSC-GSM with $N_1 = N_2 = 63$, $N_t = 7$, $N_u = 2$, $M = 4$, $N_r = 4$ and $q = 64$ is calculated as 31248. The complexity of DGRSC-SM with $N_1 = N_2 = 63$, $N_t = 16$, $M = 4$, $N_r = 4$ and $q = 64$ is computed as 30744. This reveals a mere 1.6% increase in complexity for the DGRSC-GSM over the DGRSC-SM. However, the DGRSC-GSM system achieves a 56% reduction in N_t relative to the DGRSC-SM system. Thus, it indicates that the DGRSC-GSM system enables to achieve a more favorable trade-off between performance and complexity.

The time consumption depends on specific simulation parameters. The time required for partial curves in Fig. 13 is provided: 1) For the DGRSC-GSM system with $N_t = 7$, $N_u = 2$ and $N_r = 6$, the time is 1.7 hours; 2) For the DGRSC-SM system with $N_t = 16$ and $N_r = 6$, the time is 1.65 hours. It is evident the time consumption gap between the DGRSC-GSM and DGRSC-SM systems is also relatively small.

5.6 Performance Comparison of the DGRSC-GSM and Distributed GRS Coded MIMO (DGRSC-MIMO) Systems

The BER comparison of the DGRSC-GSM and DGRSC-MIMO systems with perfect channel knowledge under the ideal *S*-*R* link at the same spectral efficiency is depicted in Fig. 14, where the traditional MIMO technique in the DGRSC-MIMO is utilized. The codes used by the *S* and *R* are $GRS_1(12, 5, 8)$ and $GRS_2(12, 3, 10)$, respectively. The OISS algorithm is adopted. For attaining the same spectral efficiency, DGRSC-GSM employs $N_t = 4$, $N_u = 2$ and BPSK ($M = 2$), while DGRSC-MIMO utilizes $N_t = 1$ and 16-QAM ($M = 16$). The simulated results show the DGRSC-GSM system outperforms the DGRSC-MIMO system when the receive antenna number N_r is the same. This indicates the use of GSM can improve the spatial diversity gain of the DGRSC-GSM system. For example, for the DGRSC-GSM and DGRSC-MIMO systems using

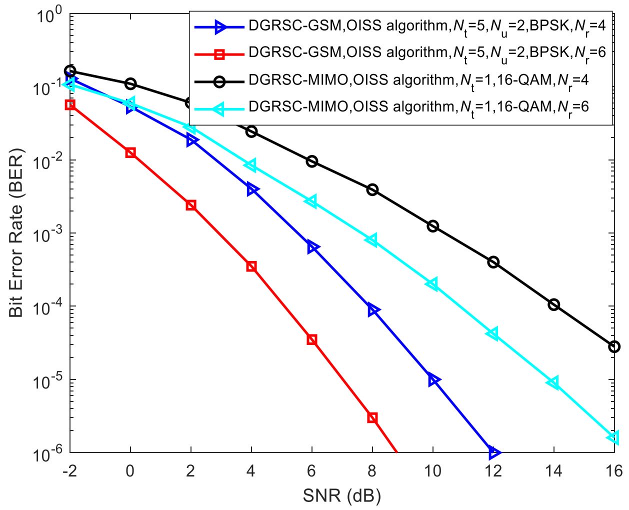

Fig. 14. Performance of the DGRSC-GSM and DGRSC-MIMO systems using $GRS_1(12,5,8)$ and $GRS_2(12,3,10)$.

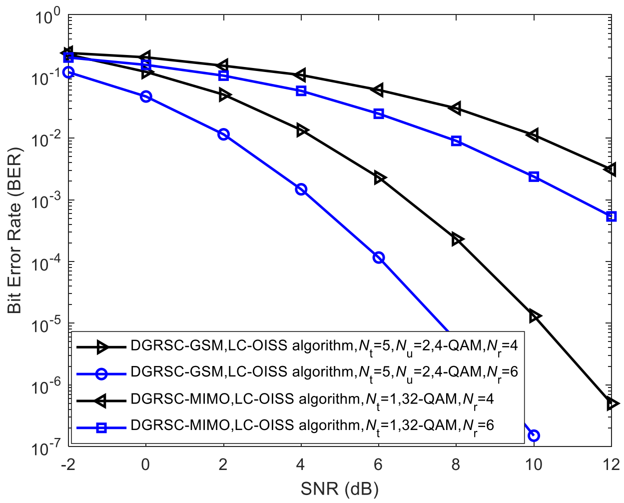

Fig. 15. Performance of the DGRSC-GSM and DGRSC-MIMO systems using $GRS_1(31,19,13)$ and $GRS_2(31,10,22)$.

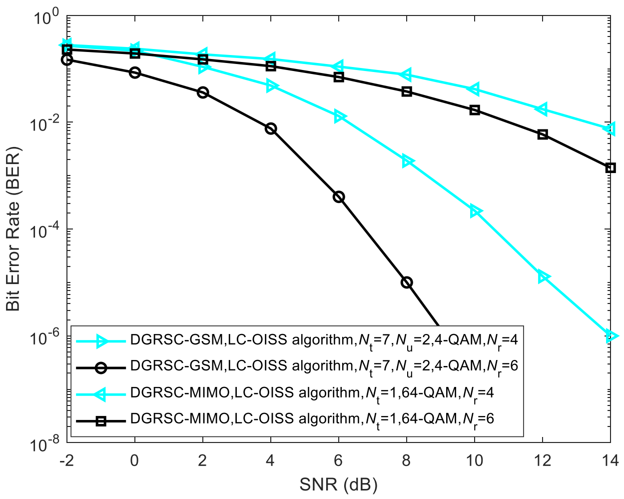

Fig. 16. Performance of the DGRSC-GSM and DGRSC-MIMO systems using $GRS_1(63,50,14)$ and $GRS_2(63,30,34)$.

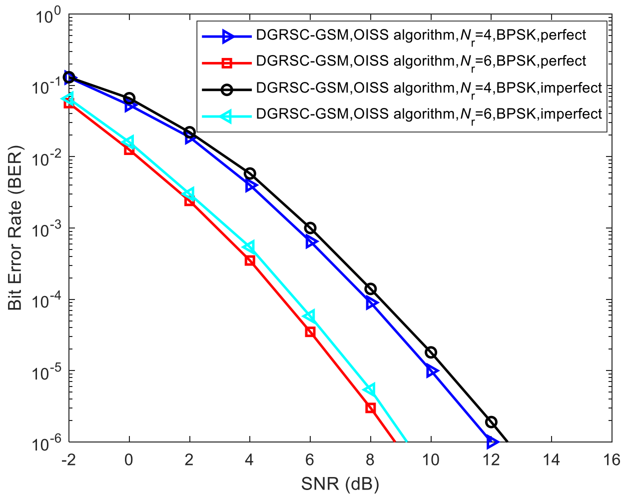

Fig. 17. Performance of the DGRSC-GSM system using $GRS_1(12,5,8)$ and $GRS_2(12,3,10)$ under perfect and imperfect channel knowledge.

$N_r = 6$, the DGRSC-GSM system at BER = 10^{-5} achieves a gain of approximately 7 dB compared to the DGRSC-MIMO system at BER = 10^{-5}. In addition, the BER performance advantage of the DGRSC-GSM system over the DGRSC-MIMO system is once again confirmed in Figs. 15 and 16. For example, in Fig. 15, the DGRSC-GSM system has an SNR gain of approximately 6.9 dB compared to the DGRSC-MIMO system at BER = 10^{-3} under $N_r = 6$.

5.7 Performance Comparison of the DGRSC-GSM System under Perfect and Imperfect Channel Knowledge

Due to the widespread presence of imperfect channel knowledge in practical communication scenarios, this subsection analyzes the performance of the DGRSC-GSM system under imperfect channel knowledge, as illustrated in Figs. 17–19. In Fig. 17, the simulation incorporates the parameters $N_t = 5$, $N_u = 2$, $M = 2$ (BPSK) and $\lambda_{S,R} = \infty$. The channel knowledge is acquired by using the optimized channel estimation method proposed in [27] and the best information symbol selection is implemented through the OISS algorithm. Simulation results demonstrate that the performance gap between perfect and imperfect channel knowledge remains minimal under the same configuration of receiving antennas. Specifically, at BER = 10^{-6}, the required SNR difference between the two channel scenarios is about 0.3 dB for $N_r = 6$. This observation in Fig. 17 indicates that employing an optimized channel estimation approach to obtain channel knowledge enables the system to attain excellent performance even under such imperfect channel conditions. Additionally, Figures 18 and 19 show the system performance for higher M-order modulations. The parameters ($N_t = 3$, $N_u = 2$, 16-QAM and $\lambda_{S,R} = \infty$) and ($N_t = 3$, $N_u = 2$, 32-QAM and $\lambda_{S,R} = \infty$) are applied in Figs. 18 and 19, respectively. The corresponding results exhibit the phenomenon analogous to that shown in Fig. 17.

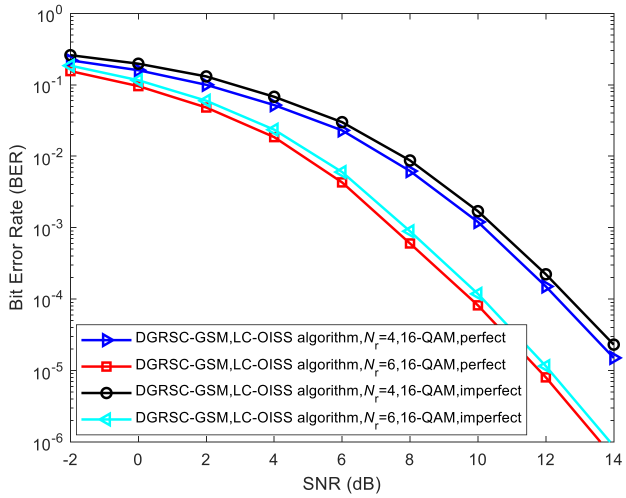

Fig. 18. Performance of the DGRSC-GSM system using $GRS_1(31,19,13)$ and $GRS_2(31,10,22)$ under perfect and imperfect channel knowledge.

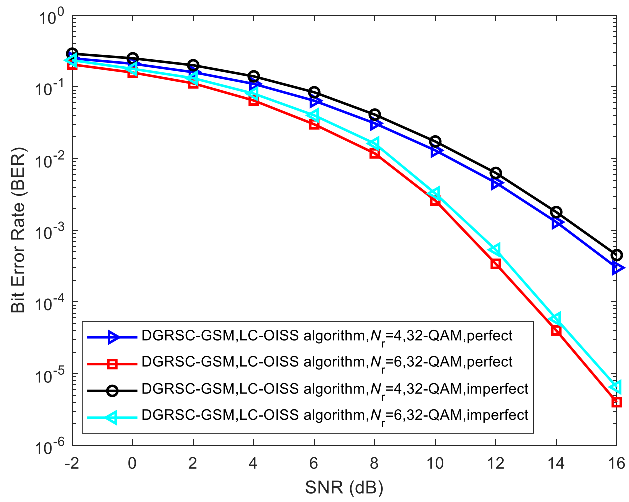

Fig. 19. Performance of the DGRSC-GSM system using $GRS_1(63,50,14)$ and $GRS_2(63,30,34)$ under perfect and imperfect channel knowledge.

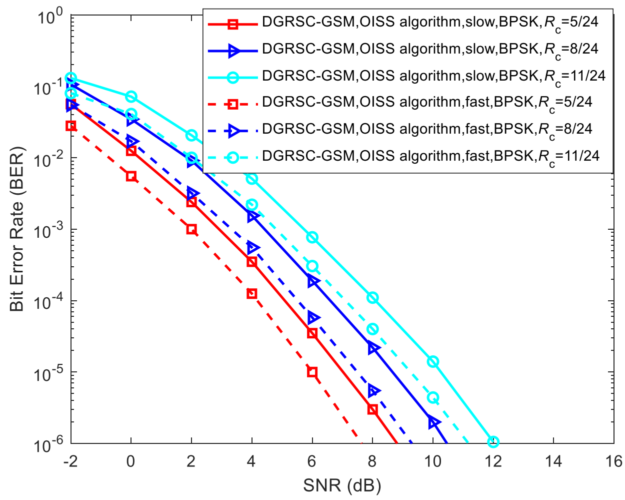

Fig. 20. Performance comparison of the DGRSC-GSM system with BPSK under varying channels and code rates.

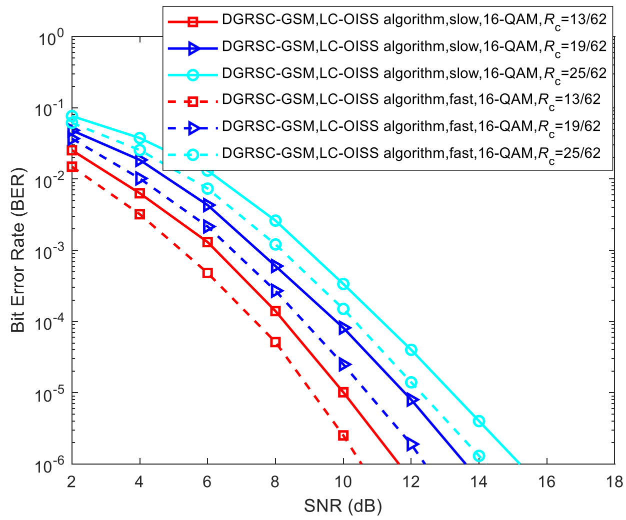

Fig. 21. Performance comparison of the DGRSC-GSM system with 16-QAM under varying channels and code rates.

5.8 Performance Comparison of the DGRSC-GSM System under Varying Channels and Code Rates

This subsection discusses the BER performance of the DGRSC-GSM system under varying channel conditions and code rates, as depicted in Figs. 20–22. The channel models include slow and fast Rayleigh fading channels. In Fig. 20, three combinations of GRS codes over GF(2^4) are taken into account: 1) $GRS_1(12, 5, 8)$ and $GRS_2(12, 3, 10)$; 2) $GRS_1(12, 8, 5)$ and $GRS_2(12, 3, 10)$; 3) $GRS_1(12, 11, 2)$ and $GRS_2(12, 3, 10)$. For the three code configurations: 1) The equivalent code rates R_c at the D are 5/24, 8/24 and 11/24, respectively; 2) The optimal information symbol selection patterns are [1, 3, 5], [2, 4, 6] and [5, 8, 10], respectively. Additionally, $N_t = 5$, $N_u = 2$, $M = 2$ (BPSK), $N_r = 6$, $\lambda_{S,R} = \infty$ and perfect channel knowledge are assumed. Results in Fig. 20 demonstrate two key observations: 1) Under identical channel conditions, the system exhibits significantly improved BER performance as the code rate decreases (from 11/24 to 5/24). This occurs because a lower code rate increases the redundant symbols, enhances the error correction capability, and ultimately strengthens the error resistance; 2) For the same code rate configuration, superior BER performance is achieved in fast fading channel compared to slow fading channel. The enhanced performance of fast fading channel can be expounded as follows: The rapid variation in the channel causes signals to experience statistically independent fading at different time instants. This independence reduces the impact of channel fading, thereby enhancing the BER performance.

The curves in Figs. 21 and 22 present the system performance with perfect channel knowledge under higher M-order modulations, exhibiting the trend similar to that observed in Fig. 20. In Figs. 21 and 22, the parameters ($N_t = 3$, $N_u = 2$, $N_r = 6$, 16-QAM and $\lambda_{S,R} = \infty$) and ($N_t = 3$, $N_u = 2$, $N_r = 6$, 32-QAM and $\lambda_{S,R} = \infty$) are utilized, respectively. The combinations of GRS codes, equivalent code rates R_c and optimized information symbol selection patterns adopted in Figs. 21 and 22 are tabulated in Tab. 3.

6. Conclusion

This article proposes the DGRSC-GSM system with information symbol selection at the R. An OISS algorithm based on complete search is designed for this system to obtain a linear block code with the optimal weight distribution at the D. To reduce the complexity of the OISS algorithm, a LC-OISS algorithm is designed. At the D, a joint decoding algorithm is designed for efficient decoding. The results show the DGRSC-GSM system using the OISS and LC-OISS algorithms possess better performance compared to that utilizing the RISS algorithm. By utilizing the LC-OISS algorithm, the performance approaches the optimal performance provided by the OISS algorithm. Compared to the non-cooperative system, the proposed DGRSC-GSM system can provide superior performance. Due to the use of GSM and optimized selection algorithm, the proposed system gets more than 2 dB over the existing systems. The results also show the proposed scheme has superior performance over the DGRSC-MIMO system. The proposed DGRSC-GSM system not only features fast encoding and decoding processes, but also achieves superior BER

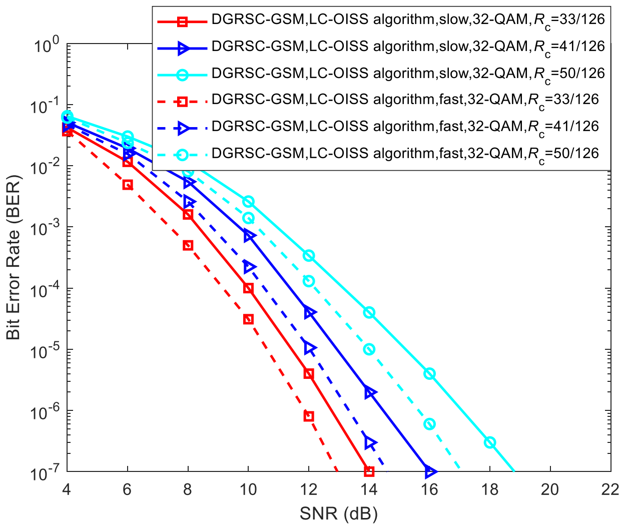

Fig. 22. Performance comparison of the DGRSC-GSM system with 32-QAM under varying channels and code rates.

Figs	$GRS_1(N_1, K_1, d_1)$ $GRS_2(N_2, K_2, d_2)$	Equivalent code rates R_c	Optimized selection patterns $p^{(low)}$
21	$GRS_1(31, 13, 19)$ $GRS_2(31, 10, 22)$	13/62	[1, 2, 3, 4, 5, 8, 9, 11, 12, 13]
	$GRS_1(31, 19, 13)$ $GRS_2(31, 10, 22)$	19/62	[1, 2, 3, 4, 6, 7, 11, 12, 13, 17]
	$GRS_1(31, 25, 7)$ $GRS_2(31, 10, 22)$	25/62	[1, 4, 6, 7, 9, 11, 14, 17, 22, 24]
22	$GRS_1(63, 33, 31)$ $GRS_2(63, 30, 34)$	33/126	[1, 3, 4, 5, 6, 7, 8, 9, 10, 11, 12, 13, 14, 15, 17, 18, 19, 20, 21, 22, 23, 24, 25, 26, 27, 29, 30, 31, 32, 33]
	$GRS_1(63, 41, 23)$ $GRS_2(63, 30, 34)$	41/126	[1, 2, 3, 4, 5, 6, 8, 10, 11, 12, 14, 15, 17, 18, 20, 21, 23, 24, 25, 26, 27, 29, 30, 31, 32, 33, 35, 36, 38, 39]
	$GRS_1(63, 50, 14)$ $GRS_2(63, 30, 34)$	50/126	[1, 3, 4, 5, 6, 7, 8, 9, 10, 11, 12, 15, 16, 20, 25, 26, 27, 28, 29, 30, 31, 32, 34, 35, 43, 46, 47, 48, 49, 50]

Tab. 3. Combinations of GRS codes, equivalent code rates R_c and optimized information symbol selection patterns of Figs. 21 and 22.

performance, making it particularly suitable for ultra-reliable low-latency communication scenarios in 5G systems. The future work will focus on designing low-complexity efficient joint decoding algorithms and developing suboptimal selection algorithms that achieve performance closer to that of the OISS algorithm.

Acknowledgments

Funding: This work was supported by Henan University of Technology High Level Talent Research Launch Foundation under the contract No. 31401676.

Data Availability Statement: All the source codes and mathematical models are available from the authors upon reasonable request.

References

[1] LIANG, H., LIU, A. J., LIU, X., et al. Construction and optimization for adaptive polar coded cooperation. *IEEE Wireless Communications Letters*, 2020, vol. 9, no. 8, p. 1187–1190. DOI: 10.1109/LWC.2020.2984738

[2] WAWERU, D. K., YANG, F. F., ZHAO, C. L., et al. Design of optimized distributed Goppa codes and joint decoding at the destination. *Telecommunication Systems*, 2022, vol. 81, no. 3, p. 341–355. DOI: 10.1007/s11235-022-00948-5

[3] ZHAO, C. L., YANG, F. F., UMAR, R., et al. Two-source asymmetric turbo-coded cooperative spatial modulation scheme with code matched interleaver. *Electronics*, 2020, vol. 9, no. 1, p. 1–20. DOI: 10.3390/electronics9010169

[4] VAN DER MEULEN, E. C. Three-terminal communication channels. *Advances in Applied Probability*, 1971, vol. 3, no. 1, p. 120–154. DOI: 10.2307/1426331

[5] LANEMAN, J. N., WORNELL, G. W., TSE, D. N. An efficient protocol for realizing cooperative diversity in wireless networks. In *Proceedings of IEEE International Symposium on Information Theory*. Washington (DC, USA), 2001, p. 294–294. DOI: 10.1109/ISIT.2001.936157

[6] LANEMAN, J. N., TSE, D. N. C., WORNELL, G. W. Cooperative diversity in wireless networks: Efficient protocols and outage behavior. *IEEE Transactions on Information Theory*, 2004, vol. 50, no. 12, p. 3062–3080. DOI: 10.1109/TIT.2004.838089

[7] HUNTER, T. E., NOSRATINIA, A. Diversity through coded cooperation. *IEEE Transactions on Wireless Communications*, 2006, vol. 5, no. 2, p. 283–289. DOI: 10.1109/TWC.2006.02006

[8] HUNTER, T. E., NOSRATINIA, A. Cooperation diversity through coding. In *Proceedings of IEEE International Symposium on Information Theory*. Lausanne (Switzerland), 2002, p. 220–220. DOI: 10.1109/ISIT.2002.1023492

[9] ALMAWGANI, A. H. M., SALLEH, M. F. M. RS coded cooperation with adaptive cooperation level scheme over multipath Rayleigh fading channel. In *Proceedings of IEEE 9th Malaysia International Conference on Communications (MICC)*. Kuala Lumpur (Malaysia), 2009, p. 480–484. DOI: 10.1109/MICC.2009.5431555

[10] ALMAWGANI, A. H. M., SALLEH, M. F. M. Coded cooperation using Reed Solomon codes in slow fading channel. *IEICE Electronics Express*, 2010, vol. 7, no. 1, p. 27–32. DOI: 10.1587/elex.7.27

[11] AL-MOLIKI, Y. M., ALDHAEEBI, M. A., ALMWALD, G. A., et al. The performance of RS and RSCC coded cooperation systems using higher order modulation schemes. In *Proceedings of the 6th International Conference on Intelligent Systems, Modelling and Simulation*. Kuala Lumpur (Malaysia), 2015, p. 211-214. DOI: 10.1109/ISMS.2015.11

[12] GUO, P. C., YANG, F. F., ZHAO, C. L., et al. Jointly optimized design of distributed Reed-Solomon codes by proper selection in relay. *Telecommunication Systems*, 2021, vol. 78, no. 3, p. 391 to 403. DOI: 10.1007/s11235-021-00822-w

[13] CHEN, C., YANG, F. F., ZHAO, C. L., et al. Distributed Reed-Solomon coded cooperative space-time labeling diversity network. *Radioengineering*, 2022, vol. 31, no. 4, p. 496–509. DOI: 10.13164/re.2022.0496

[14] ZHU, C. Z., LIAO, Q. Y. The (+)-extended twisted generalized Reed-Solomon code. *Discrete Mathematics*, 2024, vol. 347, no. 2, p. 1–18. DOI: 10.1016/j.disc.2023.113749

[15] EJAZ, S., YANG, F., XU, H. Split labeling diversity for wireless half-duplex relay assisted cooperative communication systems. *Telecommunication Systems*, 2020, vol. 75, no. 4, p. 437–446. DOI: 10.1007/s11235-020-00694-6

[16] CHEN, L., WANG, Z. Q., DU, Y., et al. Generalized transceiver beamforming for DFRC with MIMO radar and MU-MIMO communication. *IEEE Journal on Selected Areas in Communications*, 2022, vol. 40, no. 6, p. 1795–1808. DOI: 10.1109/JSAC.2022.3155515

[17] HUANG, K. Y., XIAO, Y., LIU, L. Z., et al. Integrated spatial modulation and STBC-VBLAST design toward efficient MIMO transmission. *Sensors*, 2022, vol. 22, no. 13, p. 1–14. DOI: 10.3390/s22134719

[18] YOUNIS, A., SERAFIMOVSKI, N., MESLEH, R., et al. Generalised spatial modulation. In *Conference Record of the Forty Fourth Asilomar Conference on Signals, Systems and Computers.* Pacific Grove (USA), 2010, p. 1498–1502. DOI: 10.1109/ACSSC.2010.5757786

[19] CHEN, C., YANG, F. F., WAWERU, D. K. Optimized-Goppa codes based on the effective selection of Goppa polynomials for coded-cooperative generalized spatial modulation network. *Radioengineering*, 2024, vol. 33, no. 1, p. 75–88. DOI: 10.13164/re.2024.0075

[20] ZHAO, C. L., YANG, F. F., WAWERU, D. K. Reed-Solomon coded cooperative spatial modulation based on nested construction for wireless communication. *Radioengineering*, 2021, vol. 30, no. 1, p. 172–183. DOI: 10.13164/re.2021.0172

[21] CHEN, B. C., LIU, H. W. New constructions of MDS codes with complementary duals. *IEEE Transactions on Information Theory*, 2018, vol. 64, no. 8, p. 5776–5782. DOI: 10.1109/TIT.2017.2748955

[22] CHEN, C., YANG, F. F., ZHAO, C., et al. Distributed RS coded cooperation: Optimized code construction and decoding by critical SNR aided. *Wireless Personal Communications*, 2023, vol. 132, no. 1, p. 523–548. DOI: 10.1007/s11277-023-10623-w

[23] GOVENDER, R., PILLAY, N., XU, H. J. Soft-output space-time block coded spatial modulation. *IET Communications*, 2014, vol. 8, no. 16, p. 2786–2796. DOI: 10.1049/iet-com.2014.0174

[24] WANG, J., ZHANG, S. W., MEI, Z. H., et al. RIS-assisted coded relay cooperation based on LDPC product codes with finite code length. In *Proceedings of International Conference on Wireless Communications and Signal Processing (WCSP)*. Hangzhou,

(China), 2023, p. 1038–1043. DOI: 10.1109/WCSP58612.2023.10405032

[25] PAN, Y., ZHANG, S. W. Performance analysis of RIS-assisted coded cooperation system based on polar codes with finite code length. *IEEE Signal Processing Letters*, 2024, vol. 31, p. 2290 to 2294. DOI: 10.1109/LSP.2024.3453662

[26] JUSTESEN, J. On the complexity of decoding Reed-Solomon codes. *IEEE Transactions on Information Theory*, 1976, vol. 22, no. 2, p. 237–238. DOI: 10.1109/TIT.1976.1055516

[27] ZHAO, C. L., YANG, F. F., WAWERU, D. K., et al. Distributed QC-LDPC coded spatial modulation for half-duplex wireless communications. *Radioengineering*, 2022, vol. 31, no. 3, p. 362 to 373. DOI: 10.13164/re.2022.0362

About the Authors ...

Chunli ZHAO (corresponding author) received her B.S. degree in Electronic and Information Engineering from Henan Normal University Xinlian College, China, in 2014. She obtained her M.Sc. degree in Circuits and Systems at Henan Normal University, China, in 2017. She received her Ph.D. degree in Communication and Information Systems from Nanjing University of Aeronautics and Astronautics, China, in 2024. She is currently a lecture with the College of Information Science and Engineering at Henan University of Technology. Her research interests are channel coding, coded cooperation and MIMO technique.

Fengfan YANG received the M.Sc. and Ph.D. degrees from the Northwestern Polytechnical University and South-east University, China in 1993, and 1997, respectively, all in Electronic Engineering. He has been with the College of Information Science and Technology, Nanjing University of Aeronautics and Astronautics since May 1997. From October 1999 to May 2003, he was a research associate at the Centre for Communication Systems Research, University of Surrey, UK, and Dept. of Electrical and Computer Engineering, McGill University, Canada. His major research interests are information theory, channel coding and their applications for mobile and satellite communications.

Hongjun XU (MIEEE, 07) received the B.Sc. degree from the University of Guilin Technology, Guilin, China, in 1984; the M.Sc. degree from the Institute of Telecontrol and Telemeasure, Shi Jian Zhuang, China, in 1989; and the Ph.D. degree from the Beijing University of Aeronautics and Astronautics, Beijing, China, in 1995. From 1997 to 2000, he was a Postdoctoral Fellow with the University of Natal, Durban, South Africa, and Inha University, Incheon, Korea. He is currently a full Professor with the School of Engineering at the University of KwaZulu-Natal, Durban. He is also a rated scientist of the national research foundation in South Africa. He has authored and co-authored more than 50 journal papers. His research interests include wireless communications and image processing.